Climatological Relationship between Warm Season Atmospheric Rivers and Heavy Rainfall over East Asia

Youichi KAMAE

Faculty of Life and Environmental Sciences, University of Tsukuba, Tsukuba, Japan
Scripps Institution of Oceanography, University of California San Diego, California, USA

Wei MEI

Department of Marine Sciences, University of North Carolina at Chapel Hill, North Carolina, USA

and

Shang-Ping XIE

Scripps Institution of Oceanography, University of California San Diego, California, USA

Abstract

Eddy transport of atmospheric water vapor from the tropics is important for rainfall and related natural disasters in the middle latitudes. Atmospheric rivers (ARs), intense moisture plumes that are typically associated with extratropical cyclones, often produce heavy precipitation upon encountering topography on the west coasts of mid-latitude North America and Europe. ARs also occur over the northwestern Pacific and sometimes cause floods and landslides over East Asia, but the climatological relationship between ARs and heavy rainfall in this region remains unclear. Here we evaluate the contribution of ARs to the hydrological cycle over East Asia using high-resolution daily rainfall observations and an atmospheric reanalysis during 1958−2007. Despite their low occurrence, ARs account for 14−44 % of the total rainfall and 20−90 % of extreme heavy-rainfall events during spring, summer, and autumn. AR-related extreme rainfall is especially pronounced over western-to-southeastern slopes of terrains over the Korean Peninsula and Japan, owing to strong orographic effects and a stable direction of low-level moisture flows. A strong relationship between warm-season AR heavy rainfall and preceding-winter El Niño is identified since the 1970s, suggesting the potential of predicting heavy-rainfall risk over Korea and Japan at seasonal leads.

Corresponding author: Youichi Kamae, Faculty of Life and Environmental Sciences, University of Tsukuba, 1-1-1 Tennoudai, Tsukuba, Ibaraki 305-8572, Japan
E-mail: kamae.yoichi.fw@u.tsukuba.ac.jp

1. Introduction

Meridional atmospheric circulation and large-scale atmospheric eddies advect water vapor poleward from the tropics and subtropics. The atmospheric water vapor transport is an essential component of the global hydrological cycle and energy budget (e.g., Peixoto and Oort 1992; Trenberth and Stepaniak 2003; Schneider et al. 2006). In the middle latitudes, meridional

water vapor transports by atmospheric disturbances, including tropical cyclones (e.g., Eckhardt et al. 2004; Knippertz and Wernli 2010; Boutle et al. 2011; Hawcroft et al. 2012; Newman et al. 2012), are critically important for land hydrology (e.g., heavy rainfalls) and natural disasters (e.g., droughts, floods, and landslides). Atmospheric rivers (ARs), narrow elongated water vapor plumes typically associated with extratropical cyclones, are frequently observed over the mid-latitude Northern and Southern Hemispheres (especially, over the Pacific and Atlantic Ocean; e.g., Zhu and Newell 1998; Ralph et al. 2004; Gimeno et al. 2016; American Meteorological Society 2017). ARs greatly impact water availability and natural disasters over the mid-latitude coastal regions; therefore, they have attracted much attention.

While ARs have been a focus of numerous case studies (e.g., Ralph et al. 2004, 2011; Bao et al. 2006; Stohl et al. 2008; Moore et al. 2012), their large-scale climatologies have been characterized recently using atmospheric reanalyses. Mundhenk et al. (2016) examined the basin-wide climatology and variability of the North Pacific ARs by applying an objective detection algorithm (detailed in Section 2.2). Guan and Waliser (2015) provided a global climatology of AR frequency, duration, and related rainfall for the time period of 1997–2014 using observations and an atmospheric reanalysis. Recently, Kamae et al. (2017; hereafter, K17) showed that ARs also frequently develop over the northwestern Pacific and make landfall over East Asia in addition to the west coasts of the continents as illustrated in previous studies (e.g., Ralph et al. 2004, 2006; Neiman et al. 2008; Lavers et al. 2012; Payne and Magnusdottir 2014; Gimeno et al. 2016). ARs are frequently observed over eastern China, the Korean Peninsula, and Japan especially during summer. Hirota et al. (2016) related a Hiroshima heavy-rainfall event of August 2014 to an AR-like water vapor transport from the Indochina Peninsula. Interannual variability of summertime AR occurrence (note that "AR occurrence" in this paper does not mean genesis but existence) over the northwestern Pacific is well explained by the preceding-winter El Niño through tropical atmosphere–ocean interactions and thus is highly predictable (K17; detailed below).

The role of ARs in cold season land hydrology over the west coasts of North America, Africa, and Europe has been extensively studied (e.g., Ralph et al. 2006; Neiman et al. 2008; Dettinger et al. 2011; Lavers et al. 2012; Dettinger 2013; Kim et al. 2013; Payne and Magnusdottir 2014; Lavers and Villarini 2015; Gimeno et al. 2016; Kingston et al. 2016). Over these

regions, landfalling ARs account for a large portion of the total climatological precipitation despite their limited frequency (e.g., Guan et al. 2010; Rutz et al. 2014). For example, Dettinger et al. (2011) found that AR-day rainfall accounts for 30–45 % of the total rainfall over the west coast of North America during 1998–2008. More recently, Lavers and Villarini (2015) depicted an AR contribution of a similar magnitude to the total rainfall over Western Europe and central and northeastern United States during the winter season.

While ARs may also play an important role in the warm-season (late spring to early autumn) hydrological cycle over East Asia, the extent to which ARs contribute to the total rainfall and to the occurrence of extreme heavy rainfall remains unclear. Summer is the rainy season over East Asia. Moreover, the rain-bearing East Asian summer monsoon (e.g., Ninomiya and Murakami 1987; Tao and Chen 1987; Ninomiya and Akiyama 1992; Sampe and Xie 2010) exhibits substantial seasonal-interannual variability because of the influence of both tropical forcing (e.g., the El Niño Southern Oscillation; ENSO) and extratropical atmospheric circulation (e.g., mid-latitude atmospheric teleconnections; Wu and Wang 2002; Ding et al. 2011; Kosaka et al. 2012; He et al. 2017; and references therein). In addition to typhoons from the northwestern Pacific (e.g., Mei et al. 2015; Mei and Xie 2016), a quasi-stationary Meiyu-Baiu rainband that extends from southeast China to Japan from June to mid-July is critically important for water resources and natural disasters in the regions.

Tropical climate variability, such as ENSO, strongly affects the interannual variability of the East Asian summer monsoon through the tropical western North Pacific (TWNP) anticyclone (Xie et al. 2016 and references therein). K17 found that the interannual variability of summertime AR occurrence over the northwestern Pacific is largely controlled by the preceding-winter ENSO through the Indo-western Pacific ocean capacitor (IPOC) effect (e.g., Xie et al. 2009, 2016). In a post-El Niño spring, a westward propagating ocean Rossby wave from the Pacific Ocean warms the southwest Indian Ocean. The resultant anomalous cross-equatorial winds from the north Indian Ocean result in a north Indian Ocean warming and interact with the TWNP anticyclone. While the equatorial Pacific sea surface temperature (SST) signal dissipates before summer, the warm north Indian Ocean and South China Sea and the TWNP anticyclone are robustly observed in the post-El Niño summers. The IPOC also influences warm-season East Asian climate through the South Asian High (e.g.,

Yang et al. 2007), and the Pacific–Japan (PJ) pattern (e.g., Nitta et al. 1983). Xie et al. (2016) reviewed the delayed impact of ENSO on the summertime Asian climate. Through the IPOC, the enhanced southwesterly on the northwestern flank of the TWNP anticyclone in the post-El Niño summer results in an increased occurrence of summertime ARs over eastern China and Japan (Fig. 9 in K17). Frequent summertime ARs possibly increase natural disaster risk through extreme heavy rainfalls over East Asia (e.g., Ogura et al. 1985; Kato 1998; Manda et al. 2014; Hirota et al. 2016; K17). Despite numerous case studies, the contribution of summertime ARs to extreme heavy rainfall over East Asia needs to be quantified climatologically via statistical analysis of long-term observations.

This study evaluates the role of ARs in rainfall over East Asia using high-resolution meteorological observations and reanalysis. We focus on the long-term statistics over multidecadal periods. Our results indicate that East Asian ARs contribute to large fractions of the total rainfall and extreme rainfall events during spring, summer, and autumn. AR-induced heavy rainfalls tend to occur on the western-to-southeastern slopes of the terrains over the Korean Peninsula and Japan as the direction of low-level moisture flow is relatively stable compared to typhoons. This study further identifies a strong ENSO control on interannual variability in AR-induced warm-season heavy rainfall and hence seasonal predictability.

This paper is organized as follows. Section 2 describes data and methods including an AR detection algorithm used in this study. Section 3 presents the climatology of AR rainfall and its fractional contribution to the total rainfall over East Asia. We also show a climatological heavy-rainfall map accompanied with East Asian ARs. Section 4 evaluates the effect of ENSO on interannual variability of warm-season AR-related heavy rainfall over East Asia. In Section 5, we present a summary and discussion.

2. Data and methods

2.1 Observations and reanalysis

We use the high-resolution daily precipitation datasets produced by the Asian Precipitation—Highly-Resolved Observational Data Integration Toward Evaluation of the Water Resources project (APHRODITE; Yatagai et al. 2012), developed from thousands of meteorological observation stations over Asia. This dataset has been widely used in evaluating continent-wide and regional rainfall climatology and its variability (e.g., Yasutomi et al. 2011; Peña-Arancibia et al. 2013; Ren et al. 2013; Kamae et al. 2014; Lutz et al. 2014).

We use two subsets of this dataset: APHRODITE for monsoon Asia (MA) V1101R1 at a spatial resolution of 0.5° × 0.5° and APHRODITE for Japan (APHRO JP) V1207 at a 0.05° × 0.05° resolution (Kamiguchi et al. 2010). We use these two subsets to evaluate climatology, variability, and extreme values of regional daily rainfall over East Asia (105–150°E, 20–50°N; Fig. 1a) and Japan (Fig. 1b), respectively. Note that the ending time for the 24-hour accumulation of observed precipitation differs across regions. Daily precipitation in China and Mongolia (Japan) are based on accumulation from 12UTC (15UTC) on the previous day to 12UTC (15UTC) on the day (e.g., Yatagai et al. 2012). In this study, the daily precipitation data over East Asia are compared with four time steps of six-hourly AR fields (from 18UTC on the previous day to 12UTC on the day) to composite AR-related rainfall (see Section 2.2).

We also use SST data from HadISST (e.g., Rayner et al. 2003) at a 1.0° × 1.0° spatial resolution and six-hourly (00UTC, 06UTC, 12UTC, and 18UTC) three-dimensional atmospheric fields from the Japanese Reanalysis for 55 years (JRA-55; Kobayashi et al. 2015). We use sea level pressure (SLP) and three-dimensional specific humidity and horizontal wind at a spatial resolution of 1.25° × 1.25°. These variables are used to detect AR-like features, as detailed in K17 and in Section 2.2. We focus on the time period 1958–2007, when there is an overlap between the APHRODITE and JRA-55 data.

2.2 Detection of atmospheric river and associated rainfall

We evaluate climatology, variability, and extreme values of AR-related rainfall based on the high-resolution daily rainfall dataset (Section 2.1) and detected ARs from K17. K17 applied an AR detection algorithm developed by Mundhenk et al. (2016) to three-dimensional atmospheric data derived from JRA-55. The original source code of the AR detection algorithm was provided by B. D. Mundhenk (see an appendix of Mundhenk et al. 2016). K17 used six-hourly specific humidity and horizontal wind to calculate vertically integrated water vapor transport (IVT) between 300 and 1000 hPa levels at a 1.25° × 1.25° spatial resolution. The IVT is determined as below:

$$\text{IVT} = \sqrt{\left(\frac{1}{g}\int_{1000}^{300} qu\, dp\right)^2 + \left(\frac{1}{g}\int_{1000}^{300} qv\, dp\right)^2}, \qquad (1)$$

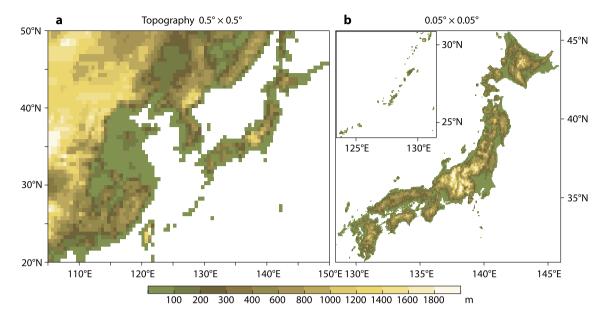where q is specific humidity, g is the acceleration due

Fig. 1.   (a) Topography (m) at spatially 0.5° × 0.5° resolution (Row et al. 1995) over East Asia and (b) at 0.05° × 0.05° resolution over Japan (distributed as a supplement of APHRO JP dataset; Kamiguchi et al. 2010). White areas indicate grid points in which APRODITE rainfall data are not available. Upper left corner of (b) represents the Ryukyu Islands.

to gravity, and u and v are zonal and meridional wind, respectively. K17 referred to the anomalous IVT field from its daily climatology (1958–2010) to exclude effects of background seasonal cycle of tropospheric water vapor content. By applying several criteria, K17 removed non-AR disturbances (e.g., tropical cyclones; see Section 5) from the six-hourly IVT field (see Fig. A2 of Mundhenk et al. 2016). First, an anomalous threshold of 140 kg m^{-1} s^{-1} was used to detect intense moisture bands. Next, IVT bands with a small area ($< 7.8 \times 10^5$ km^2) or short length ($< 1,500$ km) or small length/width ratio (< 1.325) were removed. In addition, east–west oriented IVT bands with a center of mass equatorward of 20°N were also excluded from the analysis. A temporal persistence was not included as a criterion, i.e., K17 did not examine persistence of AR events but detected AR-like features in each time step individually. The IVT-based AR detection method has been widely applied to AR predictions and climatological AR studies (e.g., Lavers et al. 2012; Nayack et al. 2014; Guan and Waliser 2015; Mundhenk et al. 2016; K17). Note that quantitative results of our study may be partly dependent on choices of AR detection criteria (see discussion in Section 5). More details of the detection method can be found in Mundhenk et al. (2016) and K17.

The JRA-55-based six-hourly AR fields at a 1.25° × 1.25° resolution are then linearly interpolated into 0.5° × 0.5° and 0.05° × 0.05° spatial resolutions and compared with land rainfall (Section 2.1) to composite AR-related rainfall (see Fig. 1c in K17). We determine that an AR exists at a given grid point on a given day if the AR is detected at least two out of four time steps (i.e., 12 h out of 24 h) from 18UTC on the previous day to 12UTC on the day. We referred these four time steps because a large part of rainfall observations over East Asia were accumulated from 12UTC (15UTC) on the previous day to 12UTC (15UTC) on the day (Section 2.1). A fractional contribution of ARs to total rainfall is derived through a comparison of rainfall accumulated during AR days to the total rainfall accumulation.

3.   Climatology of AR-related rainfall over East Asia

3.1   AR frequency and AR rainfall

ARs bring a large amount of rainfall to East Asia. Figure 2 shows the climatological seasonal-mean rainfall averaged for the days during which ARs exist at individual grid points (Section 2.2). Wintertime northeastern and western China is excluded from the
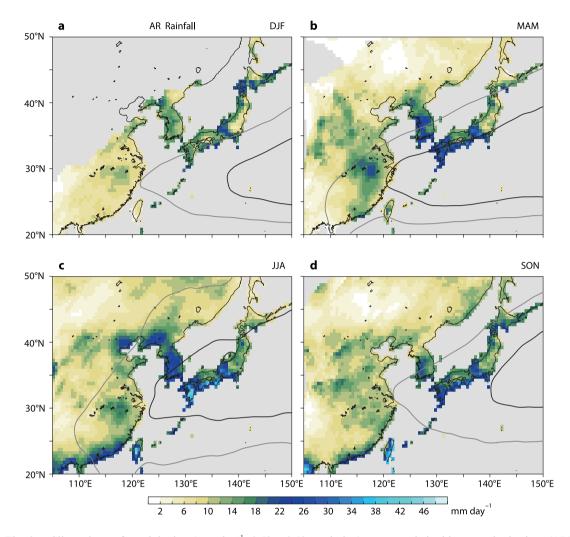
Fig. 2.   Climatology of precipitation (mm day^{-1}; 0.5° × 0.5° resolution) accompanied with atmospheric river (AR) over East Asia. (a) December-to-February (DJF), (b) March-to-May (MAM), (c) June-to-August (JJA), and (d) September-to-November (SON) mean. Gray (8 %) and black (18 %) contours represent climatology of AR frequency for 1958−2007 detected by JRA-55 vertically-integrated water vapor transport.

analysis (Fig. 2a) because of the absence of ARs. Averaged spring-to-autumn rainfall for AR days (8−44 mm day^{-1}) is much larger than climatological seasonal-mean rainfall (1−8 mm day^{-1}; e.g., Yatagai et al. 2009; Kamiguchi et al. 2010). In particular, spring-to-autumn AR rainfall is predominant over Taiwan, coastal region of southern China, the Korean Peninsula, and Japan (14−44 mm day^{-1}). Figure 3 shows higher-resolution AR rainfall maps for Japan. AR rainfall is broadly observed from southwestern to northern Japan with its peaks (18−48 mm day^{-1}) over western and central Japan from spring-to-autumn. As expected, AR rainfall exhibits a spatial pattern closely

related to topography. AR rainfall peaks are found on the western-to-southeastern slopes of mountains (Fig. 1), i.e., southern and central Kyushu, western part of the Chugoku region, southern Shikoku, southern part of the Kii Peninsula, and central and southern parts of central Japan including the Tōkai region (Fig. 3, Supplement 1). The regional correspondence between AR rainfall and terrain is also found over Taiwan (southern and eastern slopes of the Central Mountain Range), the Korean Peninsula (western slopes of the Sobaek Mountains and the Taebaek Mountains; Fig. 2, Supplement 1), and smaller mountains over Japan (the Izu Peninsula, the Abukuma Mountains, the Kitakami

Mountains, Mount Chōkai, the Shirakami Mountains, northern part of the Ou Mountains, the Oshima Peninsula, and the Hidaka Mountains; Fig. 3, Supplement 1). These results indicate strong orographic effects (see Section 3.3).

Warm-season ARs bring a large amount of rainfall especially over the Pacific coast of western and central Japan including the Tōkai region (Fig. 3). Figure 4 shows the histogram of the daily rainfall over northern Kyushu and the Tōkai region. These two regions are selected to represent the Japan Sea coast and the Pacific coast regions, respectively (see Section 3.3). Over these regions, relatively weak rainfall (< 5 mm day^{-1}) is frequent throughout the seasons while the frequency

of heavy rainfall (> 5 mm day^{-1}) is increased during spring, summer, and autumn. Histogram for AR days (orange bars in Fig. 4) is skewed to heavier rainfall than that for all days. Remarkable fractions (23−75 %) of spring-to-autumn heavy (> 20 mm day^{-1}) and extreme heavy (> 100 mm day^{-1}) rainfall are observed on AR days. The skewed histogram indicates that risk of extreme heavy rainfall greatly increases when ARs occur (see Section 3.2).

East Asian ARs contribute substantially to the climatological rainfall. Figures 5 and 6 show the fraction of AR rainfall to the seasonal total rainfall over East Asia. Despite the limited frequency (6−20 %), ARs explain a large fraction (14−44 %) of climatological
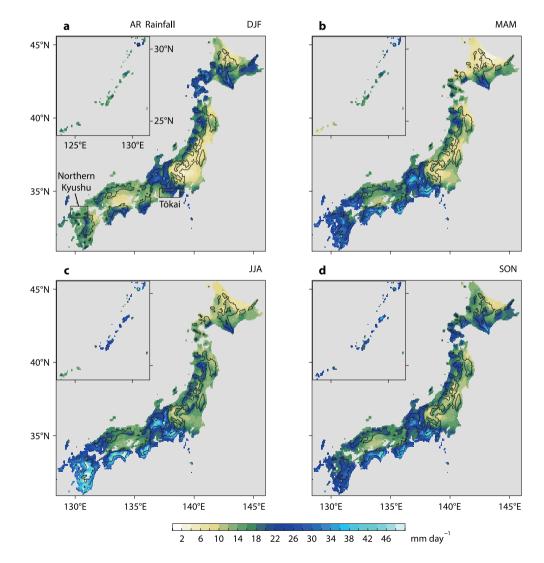

Fig. 3. Similar to Fig. 2, but for AR rainfall at spatially 0.05° × 0.05° resolution over Japan. Thin contours represent topography (400 and 1,200 m).
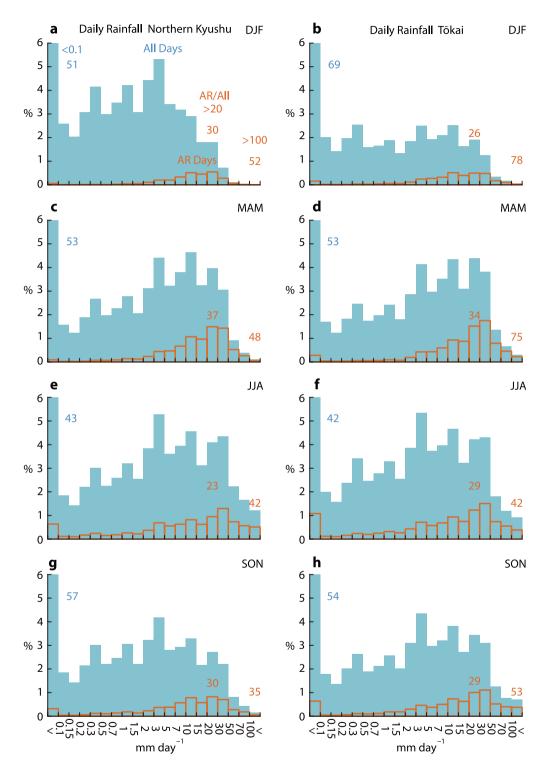
Fig. 4.   Histogram of daily rainfall for 1958–2007 over northern Kyushu region (a, c, e, g) and the Tōkai region (b, d, f, h) shown as black rectangles in Fig. 3a. Vertical axis indicates relative fraction (%). (a, b) DJF, (c, d) MAM, (e, f) JJA, and (g, h) SON. Orange bars indicate histogram of AR days. Values plotted in upper left indicate fraction (%) of no-rainfall days (< 0.1 mm day^{-1}). Two values plotted in right indicate fractions (%) of AR heavy rainfall days (> 20 mm day^{-1} and > 100 mm day^{-1}, respectively) to all heavy rainfall days.

rainfall especially over the Korean Peninsula and western Japan in spring (20−44 %; Fig. 5b). The AR contribution to total rainfall exhibits a clear seasonality largely owing to the seasonal variation of AR occurrence over the northwestern Pacific (K17). Compared to winter, springtime AR occurrence is much increased over East Asia, consistent with the increase in the AR contribution over eastern China, the Korean Peninsula, and Japan (Fig. 5b). Over the mid-latitude East Asia (30−50°N), the fractional contribution is greater in spring than in summer (Figs. 5b, c, 6b, c) despite more frequent AR occurrence in summer than in spring. In contrast to spring, the Meiyu-Baiu rainband over East Asia from June to mid-July greatly contributes to summertime rainfall over eastern China, the Korean Peninsula, and Japan with the exception

of Hokkaido. During autumn, northwestern Pacific typhoons occasionally bring heavy rainfall to East Asia (e.g., Ren et al. 2006; Prat and Nelson 2013, 2017). The dominant contributions of the Meiyu-Baiu rainband and typhoons in summer and autumn result in a lower AR contribution during these seasons compared to spring (Figs. 4, 5, 6). Over southern China, Taiwan, and the Ryukyu Islands, AR contributions are generally smaller than those at higher latitudes (30−45°N) because of lower AR frequency and more frequently approaching typhoons over these regions (20−30°N; Figs. 5, 6). Note that typhoons and ARs sometimes exhibit complex interactions over East Asia (see Section 5 and Supplement 2). In the next subsection, we examine statistical characteristics of heavy rainfall accompanied with ARs.
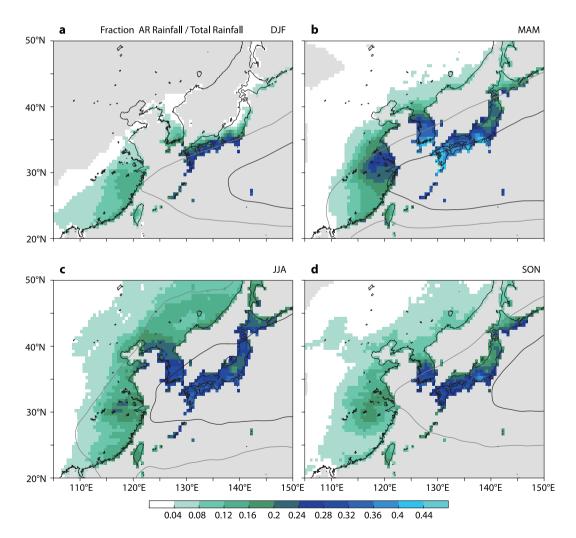

Fig. 5.   Similar to Fig. 2, but for fraction of AR rainfall to total rainfall over East Asia.

3.2 AR-related heavy rainfall

ARs over East Asia contribute to climatological seasonal-mean rainfall and increase natural disaster risk related to heavy rainfall. Figure 7 shows the frequency of extreme heavy rainfall (> 100 mm day^{-1}) accompanied with ARs over East Asia. The AR heavy rainfall is especially frequent over Taiwan, the Korean Peninsula, the Ryukyu Islands, and western and central Japan ($0.2–1.2$ %) and induces natural disasters during the warm season (K17). The heavy rainfall peaks in summer (Fig. 7c), largely consistent with the seasonal variation of the large-scale AR occurrence over East Asia (K17). In contrast, the AR heavy rainfall almost never occurs over broad areas of the Eurasian continent interior and northern part of Hokkaido during the study period (frequency of 0.02 % corresponds to only one day for the 50 years).

Similar to the mean rainfall (Fig. 3), the AR-related heavy rainfall also manifests strong effects of regional terrains. Figure 8 shows the frequency of AR heavy rainfall over Japan. Observed AR heavy rainfall over the Pacific coast of western and central Japan displays its peak in summer ($0.3–1.4$ % over Kyusyu, Shikoku, the Kii Peninsula, and central and southern parts of central Japan). In autumn, frequencies of large-scale ARs and regional AR heavy rainfall on the western slopes of mountains over western Japan (e.g., western Kyushu and western part of the Chugoku region) are
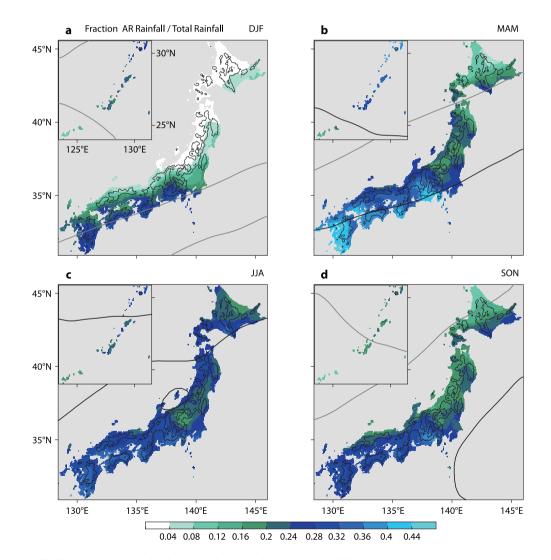

Fig. 6. Similar to Fig. 3, but for fraction of AR rainfall to total rainfall over Japan. Gray (8 %) and black (18 %) contours represent climatology of AR-day frequency for 1958–2007.
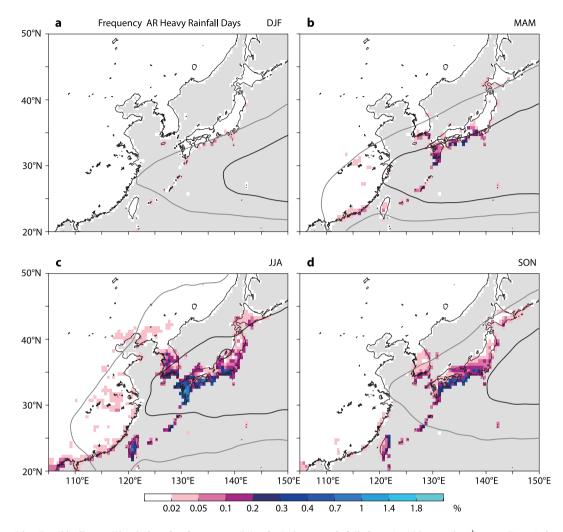
Fig. 7.   Similar to Fig. 2, but for frequency (%) of AR heavy rainfall days (> 100 mm day^{-1}) over East Asia.

greatly reduced compared to summer (Fig. 8d). In addition to western and central Japan, regional peaks are also found over northern Japan (e.g., the Kitakami Mountains, the Oshima Peninsula, and the Hidaka Mountains). The warm-season heavy rainfall on the steep terrains greatly increases the risk of natural disasters such as floods and landslides over those regions.

ARs explain a large fraction of spring-to-autumn heavy rainfall over East Asia. Figures 9 and 10 show fractions of AR heavy rainfall days to total heavy rainfall days. Despite the dominant role of typhoons in the warm-season extreme rainfall events over East Asia (e.g., Prat and Nelson 2016), ARs substantially contribute to the heavy rainfall events especially in spring and summer. During spring, 40−95 % of heavy

rainfall events over the Pacific coast of western and central Japan are observed during AR days despite the limited frequency of 18−20 % (Figs. 4d, 9b, 10b). The AR heavy rainfalls are widely observed in summer: AR days account for 20−90 % of the total heavy rainfall days over Taiwan, the Ryukyu Islands, the Korean Peninsula, and western Japan (Figs. 4e, 9c) and 50−90 % over the Pacific coast of northern Japan (e.g., the Hidaka Mountains; Fig. 10c). Occasionally approaching typhoons in autumn contribute to a large fraction of heavy-rainfall events over East Asia (Prat and Nelson 2016), resulting in a lower relative fraction of AR heavy rainfall over western Japan and the Pacific coast of northern Japan than in summer (Figs. 9d, 10d). However, 20−80 % of heavy rainfalls over the south coast of Korea and western and central
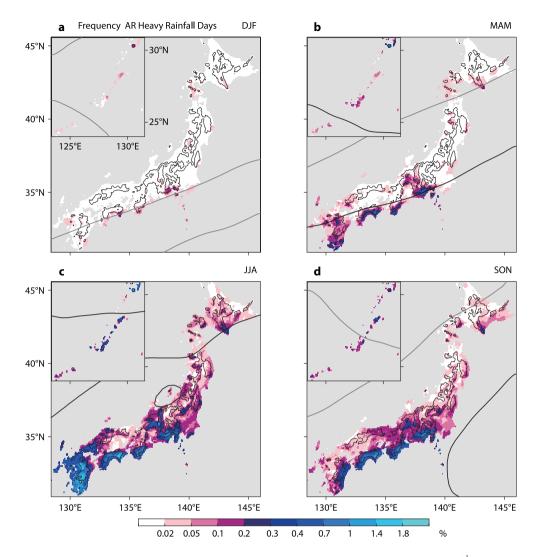
Fig. 8. Similar to Fig. 6, but for frequency (%) of AR heavy rainfall days (> 100 mm day^{-1}) over Japan.

Japan are still associated with ARs.

The above results indicate that the anomalously enhanced water vapor transports related to ARs (e.g., Fig. 1 in K17) contribute greatly to the East Asian mean and extreme rainfall. The spatial patterns of AR mean and extreme rainfall largely result from the large-scale variations of seasonal AR occurrence and regional terrains, suggesting that AR-induced natural disaster risk tends to be confined to particular regions (i.e., western-to-southeastern slopes of mountains). In the next subsection, we further examine relationships between AR-related water vapor flows, regional terrains, and AR rainfall.

3.3 Dependence of regional AR rainfall on wind direction

Over East Asia, low-level moisture flows accompanied with ARs possibly induce heavy rainfall when they encounter the meridionally running mountains over the Korean Peninsula and Japan (Fig. 1). From a geographical view, the mountains over Japan elongated in the southwest–northeast direction (Fig. 1b) strongly affect the climatological spatial patterns of rainfall and snowfall (e.g., cold northwesterly associated with the East Asian winter monsoon induces a large amount of snowfall on the western slopes of mountains over Japan, e.g., Manabe 1958; Ninomiya 1968; Ueda et al. 2015). In this section, we examine which direction of low-level wind is responsible for
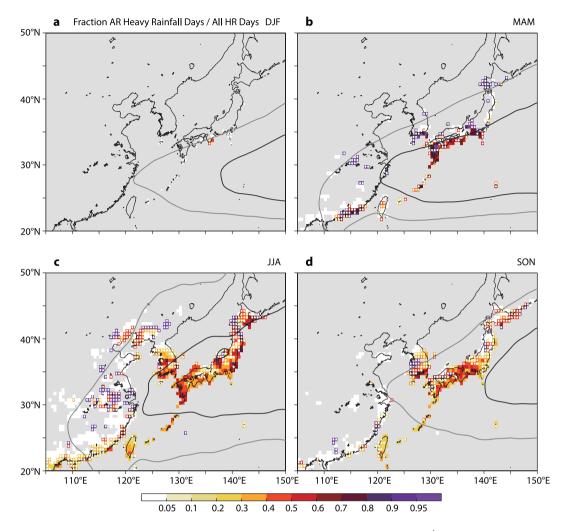
Fig. 9.   Similar to Fig. 2, but for fraction of AR heavy rainfall days (> 100 mm day^{-1}) to all heavy rainfall days over East Asia. White stipples indicate grid points with limited sample sizes (frequency of AR heavy rainfall days < 0.08 %; Fig. 7).

the regional AR rainfall over Japan (Section 2.1). Figures 11a, 11c, 11e, and 11g show spatial patterns of weighted-mean wind direction contributing to regional AR rainfall. The wind direction is derived as follows:

$$\left(\frac{\sum p_{AR} u_{AR}}{\sum p_{AR}}, \frac{\sum p_{AR} v_{AR}}{\sum p_{AR}} \right), \qquad (2)$$

where u and v is the large-scale daily-mean zonal and meridional wind from JRA-55 averaged between 800 and 1000 hPa levels, and p is the daily precipitation from APHRO JP. Subscript of AR indicates those of AR days. The atmospheric variables from JRA-55 were linearly interpolated into a 0.05° × 0.05° resolu-

tion before any further analyses. Note that u and v indicate a large-scale atmospheric circulation field. The resultant wind vector of Eq. (2) indicates a dominant large-scale low-level wind field accompanied with regional AR rainfall. Spatial patterns of the wind direction shown in Figs. 11c, 11e, and 11g are closely related to regional terrains, i.e., a westerly-to-southwesterly wind favors spring, summer, and autumn AR rainfall over western Kyushu and the Japan Sea coast, whereas a southwesterly-to-southerly wind promotes AR rainfall over eastern Kyushu and the Pacific coast of western, central, and northern Japan. The wind direction map shown in Figs. 11c, 11e, and 11g can be clearly divided into two AR rainfall regimes: the
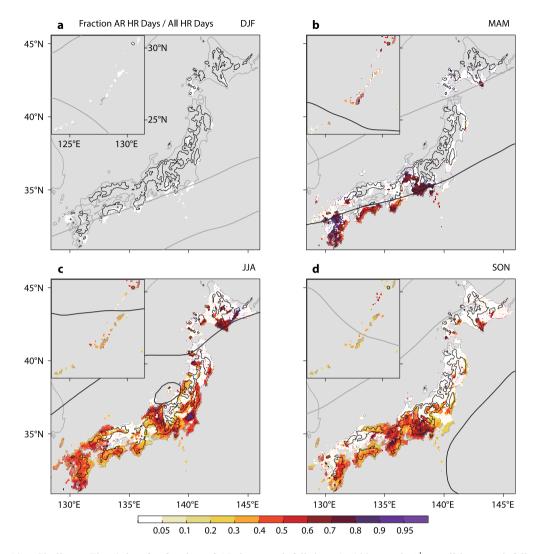
Fig. 10.   Similar to Fig. 6, but for fraction of AR heavy rainfall days (> 100 mm day^{-1}) to all heavy rainfall days over Japan. White stipples indicate grid points with limited sample sizes (frequency of AR heavy rainfall days < 0.08 %; Fig. 8).

Japan Sea coast region (westerly regime) and the Pacific coast region (southerly regime).

Low-level moisture flows accompanied with East Asian ARs are mostly in the westerly-to-southerly directions (e.g., Hirota et al. 2016; K17). Therefore, the wind direction accompanied with AR heavy rainfall is quite stable during spring, summer, and autumn (Figs. 11c, e, g). Such a wind–rainfall relationship is distinct from that related to non-AR rainfall events. Figures 11b, 11d, 11f, and 11h show the wind direction map associated with all rainfall events instead of AR events. The wind direction is derived as below:

$$\left(\frac{\sum pu}{\sum p}, \frac{\sum pv}{\sum p}\right).$$ (3)

The summertime wind direction map (Fig. 11f) is similar to Fig. 11e, while other seasons exhibit different patterns. In winter, cold northwesterly from the Eurasian continent associated with the East Asian winter monsoon absorbs a large amount of moisture from the Japan Sea (Manabe 1958; Ninomiya 1968; Ueda et al. 2015). The modified air mass induces a heavy rainfall and snowfall (Fig. 11b), greatly contributing to the seasonal-mean climatological precipitation
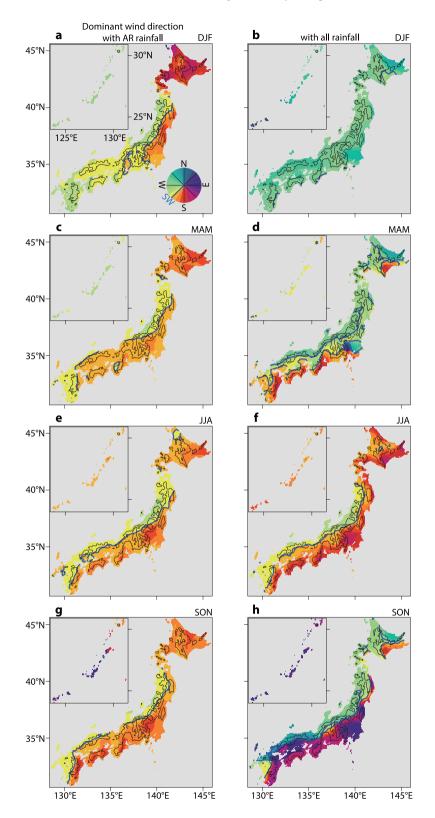
Fig. 11. Seasonal dominant wind direction accompanied with (a, c, e, g) AR rainfall and (b, d, f, h) rainfall for all days over Japan. Blue lines indicate southwesterly direction. (a, b) DJF, (c, d) MAM, (e, f) JJA, and (g, h) SON.

over Japan. Over western and eastern Japan, occasionally approaching typhoons produce heavy rainfalls especially in autumn. Northwestward-to-westward moving rainbands in the north part of typhoons bring heavy rainfall to western and eastern Japan especially on eastern and southern slopes of mountains (Fig. 11h). The great contribution of southeasterly wind is also found on eastern slopes of mountains over the Pacific coast of western Japan in spring and summer (Figs. 11d, f).
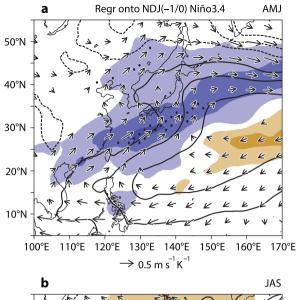
The above results suggest that natural disaster risk related to AR heavy rainfall is especially high over the western-to-southeastern slopes of mountains (Figs. 7, 8) owing to the associated stable moisture flow in contrast to highly variable wind directions accompanied with other disturbances including typhoons. Therefore, anomalously high risk of floods and landslides due to AR heavy rainfall would be predicable if we could accurately predict variations of the East Asian AR frequency and intensity. In the next section, we examine the interannual variability of AR heavy rainfall over East Asia, and the physical relationship with AR frequency and ENSO variability.

4. Interannual variability

4.1 Anomalous AR frequency in post-El Niño summer over East Asia

The anomalously intense moisture flow accompanied with the spring-to-autumn AR brings heavy rainfall to East Asia, especially over the Korean Peninsula and Japan. The seasonal-mean frequency of heavy-rainfall events can vary substantially because of variations in large-scale AR fields. K17 found that summertime AR occurrence over East Asia is strongly affected by eastern equatorial Pacific SST anomalies during the preceding winter through the atmospheric circulation anomalies over the TWNP and East Asia. In the post-El Niño summer, anomalous anticyclone over the TWNP favored by the IPOC effect (Section 1) enhances low-level southwesterly on the northwestern flank of anticyclone and increases occurrence of ARs over eastern China, the Korean Peninsula, and Japan. However, the western North Pacific response to El Niño forcing is not seasonally uniform from spring-to-autumn. This section examines seasonally asymmetric response of East Asian atmospheric circulation and AR activity in post-El Niño spring-to-autumn.

Figure 12 shows the regression of East Asian atmospheric circulation in late spring (April–May–June; AMJ) and late summer (July–August–September; JAS) onto the preceding-winter (November–December–January; NDJ) Niño3.4 (5°S–5°N, 170–120°W)
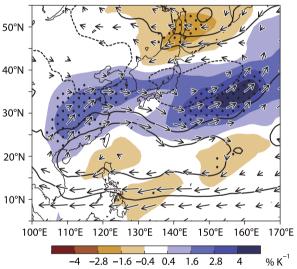

Fig. 12. Spatial patterns of regression coefficients of (a) April–May–June (AMJ) and (b) July–August–September (JAS) AR frequency (shading; % K^{-1}), sea level pressure (SLP; contour; ± 0.2, 0.4, 0.6 hPa K^{-1}), and horizontal wind at the 850 hPa level (vector; m s^{-1} K^{-1}) in JRA-55 (for 1979–2007) with preceding-winter (November–December–January; NDJ) Niño3.4 (5°S–5°N, 170–120°W) SST. Solid and dashed contours represent positive and negative SLP, respectively. Five-year high pass filter was applied before the analyses. Stipples indicate the areas with 95 % statistical confidence for anomaly of AR frequency.

index during 1979–2007. Supplement 3 provides regression map for an earlier period. The anomalous TWNP anticyclone persists from spring to summer although the equatorial Pacific SST anomalies dissipate before summer. From El Niño winter to spring, anomalous northeasterly enhances wind speed over the TWNP region, resulting in a local Wind-Evaporation-SST (WES) feedback (Xie and Philander 1994) that sustains the positive SLP anomaly (Wang et al. 2000). The SLP anomaly in AMJ favors the southwesterly anomaly on the northwestern flank of the anticyclone including eastern China and Japan, thus increasing water vapor transport and frequency of AR (Fig. 12a). In summer, East Asian atmospheric circulation is affected by warm SST anomalies in the North Indian Ocean and the East China Sea. Eastward-propagating Kelvin waves from the warm Indian Ocean favors an anomalous TWNP anticyclone in post-El Niño summer (Fig. 12b; Xie et al. 2009) despite an absence of the eastern equatorial Pacific SST forcing. The summertime positive SLP anomaly and suppressed convective activity around the Philippines (15–20°N) favor the PJ pattern (Nitta 1987): negative and positive SLP anomalies over Japan (35°N) and the Okhotsk Sea (55°N), respectively (Fig. 12b). In contrast to late spring (Fig. 12a), the PJ pattern dominates in summer because of the prevailing monsoon westerly that is a necessary condition for the atmospheric teleconnection (Kosaka et al. 2013; Xie et al. 2016). The meridional SLP gradient between 20°N and 35°N results in southwesterly anomalies over eastern China, Korea, and the south of Japan (Fig. 12b). The enhanced southwesterly moisture transport has recently been related to increased rainfall in mountainous central China in post-El Niño summers (Hu et al. 2017). The anomalous southwesterly winds favor AR occurrence over the mid-latitude East Asia except the Pacific coast of western Japan where northwesterly wind anomalies prevail (Fig. 12b). In the next subsection, we further examine relationship between ENSO and occurrence of regional AR heavy rainfall.

4.2 AR-related heavy rainfall in post-El Niño summer

The post-El Niño atmospheric circulation and AR frequency over East Asia shown above also affect regional heavy rainfall occurrence. Figure 13 shows anomalies in frequency of AR heavy-rainfall events (> 100 mm day^{-1}) in post-El Niño spring and summer. The spatial pattern of AR heavy-rainfall frequency are largely consistent with those of AR frequency: large positive anomalies over the Pacific coast of western Japan in AMJ (Figs. 13a, b) and on the western slope

of the Taebaek Mountains on the Korean Peninsula and the Japan Sea coast of western and central Japan in JAS (Figs. 13c, d). The anomalous southwesterly over the Ryukyu Islands and the Pacific coast of western Japan in AMJ favors occurrences of ARs (1.6–3.0 % K^{-1}) and AR heavy rainfall (0.1–0.5 % K^{-1}; statistically significant over the Ryukyu Islands, southern Kyushu, southeastern Shikoku and southern part of the Kii Peninsula; Figs. 13a, b). Positive anomalies in AR frequency are broadly found over East Asia, while the statistically significant anomaly in AR heavy rainfall occurrence is limited to narrow regions. Over the Japan Sea coast, the AR-related low-level westerly is responsible for the AR heavy rainfall (Fig. 11). The southerly-to-southeasterly anomaly in AMJ (Fig. 12a) is not favorable for heavy rainfall over this region (Figs. 13a, b). A statistically significant increase in AR heavy-rainfall frequency (0.05 % K^{-1}) is found over the Oshima Peninsula although the positive AR frequency anomaly is smaller than that over the lower latitudes.

The tripole SLP pattern in JAS results in more complex patterns of low-level circulation and AR frequency than in AMJ (Fig. 12), leading to a distinct pattern of AR heavy rainfall occurrence. The large positive anomaly in AR heavy-rainfall frequency (0.1–0.4 % K^{-1}), statistically significant over the Japan Sea coast of western and central Japan (Figs. 13c, d), is largely consistent with the predominant positive anomaly in the large-scale AR frequency over the middle latitude (35°N). Over the Pacific coast of western Japan, the southerly wind anomaly is responsible for the anomalous heavy rainfall (Fig. 11e). The low-level northwesterly anomaly in JAS (Fig. 12b) is not instrumental in increasing the frequency of AR and AR heavy rainfall (Figs. 13c, d). These results suggest that the anomalous occurrence of warm-season heavy rainfall accompanied with ARs is largely explained by the response of the East Asian atmospheric circulation to preceding-winter ENSO forcing, therefore possibly predictable. Note that increasing AR heavy rainfall over central and eastern Hokkaido in JAS (0.02–0.1 % K^{-1}) is not simply explained by the large-scale AR frequency and low-level circulation (easterly anomaly). Anomalously intense ARs with limited frequency may contribute to this anomalous heavy rainfall.

5. Summary and discussion

This study examines the climatology of AR-related rainfall and extreme heavy-rainfall events over East Asia. Despite their limited occurrence, ARs bring a
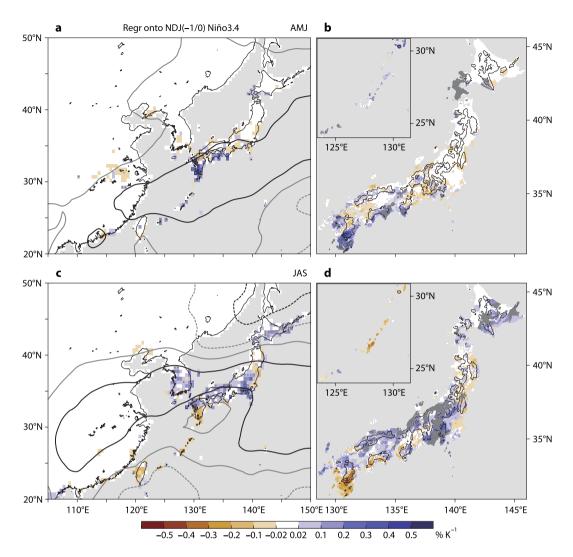
Fig. 13.   Spatial patterns of regression coefficients of (a) AMJ and (c) JAS frequency of AR heavy rainfall days (shading; % K^{-1}) and AR frequency (contour; gray indicates ± 0.4 % K^{-1}, black indicates ± 1.6 % K^{-1}) over East Asia with preceding-winter (NDJ) Niño3.4 SST. Solid and dashed contours represent positive and negative anomaly, respectively. Five-year high pass filter was applied before the analyses. (b, d) Similar to (a, c), but for Japan. Stipples indicate the areas with 95 % statistical confidence.

large amount of rainfall to East Asia, and account for 14–44 % of spring-to-autumn rainfall over Taiwan, coastal region of southern China, the Korean Peninsula, and western and central Japan. Regional mountains over East Asia exert strong orographic effects, resulting in much more AR heavy rainfall on the western-to-southeastern slopes than the eastern-to-northern slopes owing to prevailing westerly-to-southerly low-level moisture flows. In particular, the East Asian ARs explain 20–90 % of spring-to-autumn heavy-rainfall events over Taiwan, the Ryukyu

Islands, the Korean Peninsula, and western and central Japan. Risk hotspots for AR-related natural disasters are confined to narrow regions because of the stable wind direction, unlike those induced by other synoptic disturbances including typhoons. The large interannual variations of warm-season AR occurrence and low-level atmospheric circulation over East Asia related to ENSO induce anomalously frequent heavy rainfall over the Korean Peninsula and Japan. In post-El Niño spring, anomalous southwesterlies from the tropics increases the frequency of AR-related heavy

rainfall over the Pacific coasts of western Japan. In late summer, the PJ pattern and associated low-level flow reduce the frequency of AR heavy rainfall over the Pacific coasts of western Japan but increase it over the Korean Peninsula and the Japan Sea coasts of western and central Japan. The strong coupling between ENSO and the stable wind direction sheds light on the predictability of anomalous natural disaster risk due to warm-season AR activity over East Asia.

The quantitative results for the climatology of AR rainfall and its relative contribution to total rainfall may be partly dependent on AR detection methods. A variety of detection methods have been proposed in previous studies (e.g., Gimeno et al. 2014): percentile-based (e.g., Lavers et al. 2012; Nayack et al. 2014) or fixed IVT criterion (e.g., Rutz et al. 2014; Mundhenk et al. 2016) with various other criteria, including length, length/width ratio, and orientation of moisture flow. These differences may quantitatively affect the results. Guan and Waliser (2015) compared AR features detected on the basis of different methods and concluded that the results are similar but sensitive to a particular criterion (such as length of detected feature). Mundhenk et al. (2016) showed similar climatology of North Pacific AR occurrence as in Guan and Waliser (2015) although they employed different detection methods and used different atmospheric datasets. These results suggest that the AR contribution to warm-season heavy rainfall over East Asia and its interannual variability examined in this study should be qualitatively similar when a different method is adopted. It is also important to evaluate effects of transitioning tropical cyclones and remote impacts of typhoons to East Asian rainfall (e.g., Galarneau et al. 2010; Yoshida and Itoh 2012; Hirata and Kawamura 2014; see Supplement 2) although we excluded direct impact of typhoons (Sections 2.2 and 3.3). Further studies on the interactions of large-scale East Asian monsoon, ARs, typhoons, and tropical and mid-latitude climate variabilities are needed to improve our understanding of East Asian heavy rainfall and its seasonal predictability.

K17 showed that variations in summertime AR occurrence over the northwestern Pacific are largely explained by the preceding-winter ENSO variability and have high predictability. Our results further reveal that the occurrence of spring-to-autumn heavy rainfall accompanied with ARs is also closely related to the preceding-winter ENSO, and the relationship is seasonally asymmetric between spring and summer. In addition, regional variability of AR heavy rainfall occurrence is largely controlled by AR occurrence

and low-level wind direction relative to East Asian terrains. In this study, we focus only on the relationship between AR-related heavy rainfall and ENSO after 1979. The coupling between East Asian climate and ENSO varies on interdecadal time scales (e.g., Xie et al. 2010; Kubota et al. 2016), resulting in a distinct pattern of anomaly in AR occurrence for the period prior to the 1970s (Supplement 3). Further investigations on interdecadal variability of tropical atmosphere–ocean interactions and associated teleconnections are needed for more reliable predictions of risk of AR-related natural disasters over the mid-latitude East Asia.

Supplements

Supplement 1 provides geographical names over the Korean Peninsula and Japan used in this study. Supplement 2 shows examples of local and remote effects of typhoons on East Asian ARs. Supplement 3 provides discussion on interdecadal variability of the East Asian AR–ENSO coupling.

Acknowledgments

References

American Meteorological Society, 2017: Atmospheric river. *Glossary of Meteorology*. Amer. Meteor. Soc. [Available at http://glossary.ametsoc.org/wiki/Atmospheric_river.]

Bao, J.-W., S. A. Michelson, P. J. Neiman, F. M. Ralph, and J. M. Wilczak, 2006: Interpretation of enhanced integrated water vapor bands associated with extratropical cyclones: Their formation and connection to tropical moisture. *Mon. Wea. Rev.*, **134**, 1063–1080.

Boutle, I. A., S. E. Belcher, and R. S. Plant, 2011: Moisture transport in midlatitude cyclones. *Quart. J. Roy. Meteor. Soc.*, **137**, 360–373.

Dettinger, M. D., 2013: Atmospheric rivers as drought busters on the U.S. West Coast. *J. Hydrometeor.*, **14**, 1721–1732.

Dettinger, M. D., F. M. Ralph, T. Das, P. J. Neiman, and D. R. Cayan, 2011: Atmospheric rivers, floods, and the water resources of California. *Water*, **3**, 445–478.

Ding, Q., B. Wang, J. M. Wallace, and G. Branstator, 2011: Tropical-extratropical teleconnections in boreal summer: Observed interannual variability. *J. Climate*,

24, 1878–1896.

Eckhardt, S., A. Stohl, H. Wernli, P. James, C. Forster, and N. Spichtinger, 2004: A 15-year climatology of warm conveyor belts. *J. Climate*, **17**, 218–237.

Galarneau, Jr., T. J., L. F. Bosart, and R. S. Schumacher, 2010: Predecessor rain events ahead of tropical cyclones. *Mon. Wea. Rev.*, **138**, 3272–3297.

Gimeno, L., R. Nieto, M. Vázquez, and D. A. Lavers, 2014: Atmospheric rivers: A mini-review. *Front. Earth Sci.*, **2**, 2.1–2.6.

Gimeno, L., F. Dominguez, R. Nieto, R. Trigo, A. Drumond, C. J. C. Reason, A. S. Taschetto, A. M. Ramos, R. Kumar, and J. Marengo, 2016: Major mechanisms of atmospheric moisture transport and their role in extreme precipitation events. *Ann. Rev. Environ. Res.*, **41**, 117–141.

Guan, B., and D. E. Waliser, 2015: Detection of atmospheric rivers: Evaluation and application of an algorithm for global studies. *J. Geophys. Res.*, **120**, 12514–12535.

Guan, B., N. P. Molotch, D. E. Waliser, E. J. Fetzer, and P. J. Neiman, 2010: Extreme snowfall events linked to atmospheric rivers and surface air temperature via satellite measurements. *Geophys. Res. Lett.*, **37**, L20401, doi:10.1029/2010GL044696.

Hawcroft, M. K., L. C. Shaffrey, K. I. Hodges, and H. F. Dacre, 2012: How much Northern Hemisphere precipitation is associated with extratropical cyclones? *Geophys. Res. Lett.*, **39**, L24809, doi:10.1029/2012GL053866.

He, S., Y. Gao, F. Li, H. Wang, and Y. He, 2017: Impact of Arctic Oscillation on the East Asian climate: A review. *Earth Sci. Rev.*, **164**, 48–62.

Hirata, H., and R. Kawamura, 2014: Scale interaction between typhoons and the North Pacific subtropical high and associated remote effects during the Baiu/Meiyu season. *J. Geophys. Res.*, **119**, 5157–5170.

Hirota, N., Y. N. Takayabu, M. Kato, and S. Arakane, 2016: Roles of an atmospheric river and a cutoff low in the extreme precipitation event in Hiroshima on 19 August 2014. *Mon. Wea. Rev.*, **144**, 1145–1160.

Hu, K., S.-P. Xie, and G. Huang, 2017: Orographically-anchored El Niño effect on summer rainfall in central China. *J. Climate*, in press, doi:10.1175/JCLI-D-17-0312.1.

Kamae, Y., M. Watanabe, M. Kimoto, and H. Shiogama, 2014: Summertime land-sea thermal contrast and atmospheric circulation over East Asia in a warming climate–Part I: Past changes and future projections. *Climate Dyn.*, **43**, 2553–2568.

Kamae, Y., W. Mei, S.-P. Xie, M. Naoi, and H. Ueda, 2017: Atmospheric rivers over the Northwestern Pacific: Climatology and interannual variability. *J. Climate*, **30**, 5605–5619.

Kamiguchi, K., O. Arakawa, A. Kitoh, A. Yatagai, A. Hamada, and N. Yasutomi, 2010: Development of APHRO_JP, the first Japanese high-resolution daily precipitation product for more than 100 years. *Hydro. Res. Lett.*, **4**, 60–64.

Kato, T., 1998: Numerical simulation of the band-shaped torrential rain observed over southern Kyushu, Japan on 1 August 1993. *J. Meteor. Soc. Japan*, **76**, 97–128.

Kim, J., D. E. Waliser, P. J. Neiman, B. Guan, J.-M. Ryoo, and G. A. Wick, 2013: Effects of atmospheric river landfalls on the cold season precipitation in California. *Climate Dyn.*, **40**, 465–474.

Kingston, D. G., D. A. Lavers, and D. M. Hannah, 2016: Floods in the Southern Alps of New Zealand: The importance of atmospheric rivers. *Hydrol. Processes*, **30**, 5063–5070.

Knippertz, P., and H. Wernli, 2010: A Lagrangian climatology of tropical moisture exports to the Northern Hemispheric extratropics. *J. Climate*, **23**, 987–1003.

Kobayashi, S., Y. Ota, Y. Harada, A. Ebita, M. Moriya, H. Onda, K. Onogi, H. Kamahori, C. Kobayashi, H. Endo, K. Miyaoka, and K. Takahashi, 2015: The JRA-55 Reanalysis: General specifications and basic characteristics. *J. Meteor. Soc. Japan*, **93**, 5–48.

Kosaka, Y., J. S. Chowdary, S.-P. Xie, Y.-M. Min, and J.-Y. Lee, 2012: Limitations of seasonal predictability for summer climate over East Asia and the Northwestern Pacific. *J. Climate*, **25**, 7574–7589.

Kosaka, Y., S.-P. Xie, N.-C. Lau, and G. A. Vecchi, 2013: Origin of seasonal predictability for summer climate over the Northwestern Pacific. *Proc. Natl. Acad. Sci. USA*, **110**, 7574–7579.

Kubota, H., Y. Kosaka, and S.-P. Xie, 2016: A 117-year long index of the Pacific-Japan pattern with application to interdecadal variability. *Int. J. Climatol.*, **36**, 1575–1589.

Lavers, D. A., and G. Villarini, 2015: The contribution of atmospheric rivers to precipitation in Europe and the United States. *J. Hydrol.*, **522**, 382–390.

Lavers, D. A., G. Villarini, R. P. Allan, E. F. Wood, and A. J. Wade, 2012: The detection of atmospheric rivers in atmospheric reanalyses and their links to British winter floods and the large-scale climatic circulation. *J. Geophys. Res.*, **117**, D20106, doi:10.1029/2012JD018027.

Lutz, A. F., W. W. Immerzeel, A. B. Shrestha, and M. F. P. Bierkens, 2014: Consistent increase in High Asia's runoff due to increasing glacier melt and precipitation. *Nat. Climate Change*, **4**, 587–592.

Manabe, S., 1958: On the estimation of energy exchange between the Japan Sea and the atmosphere during winter based upon the energy budget of both the atmosphere and the sea. *J. Meteor. Soc. Japan*, **36**, 123–134.

Manda, A., H. Nakamura, N. Asano, S. Iizuka, T. Miyama, Q. Moteki, M. K. Yoshioka, K. Nishii, and T. Miyasaka, 2014: Impacts of a warming marginal sea on torrential rainfall organized under the Asian summer monsoon. *Sci. Rep.*, **4**, 5741, doi:10.1038/srep05741.

Mei, W., and S.-P. Xie, 2016: Intensification of landfalling typhoons over the Northwest Pacific since the late

1970s. *Nat. Geosci.*, **9**, 753–757.

Mei, W., S.-P. Xie, M. Zhao, and Y. Wang, 2015: Forced and internal variability of tropical cyclone track density in the western North Pacific. *J. Climate*, **28**, 143–167.

Moore, B. J., P. J. Neiman, F. M. Ralph, and F. E. Barthold, 2012: Physical processes associated with heavy flooding rainfall in Nashville, Tennessee, and vicinity during 1–2 May 2010: The role of an atmospheric river and mesoscale convective systems. *Mon. Wea. Rev.*, **140**, 358–378.

Mundhenk, B. D., E. A. Barnes, and E. D. Maloney, 2016: All-season climatology and variability of atmospheric river frequencies over the North Pacific. *J. Climate*, **29**, 4885–4903.

Nayak, M. A., G. Villarini, and D. A. Lavers, 2014: On the skill of numerical weather prediction models to forecast atmospheric rivers over the central United States. *Geophys. Res. Lett.*, **41**, 4354–4362.

Neiman, P. J., F. M. Ralph, G. A. Wick, J. D. Lundquist, and M. D. Dettinger, 2008: Meteorological characteristics and overland precipitation impacts of atmospheric rivers affecting the west coast of North America based on eight years of SSM/I satellite observations. *J. Hydrometeor.*, **9**, 22–47.

Newman, M., G. N. Kiladis, K. M. Weickmann, F. M. Ralph, and P. D. Sardeshmukh, 2012: Relative contributions of synoptic and low-frequency eddies to time-mean atmospheric moisture transport, including the role of atmospheric rivers. *J. Climate*, **25**, 7341–7361.

Ninomiya, K., 1968: Heat and water budget over the Japan Sea and the Japan Islands in winter season. *J. Meteor. Soc. Japan*, **46**, 343–372.

Ninomiya, K., and T. Murakami, 1987: The early summer rainy season (Baiu) over Japan. *Monsoon Meteorology*. Chang, C.-P., and T. N. Krishnamurti (eds.), Oxford University Press, Oxford, 93–121.

Ninomiya, K., and T. Akiyama, 1992: Multiscale features of Baiu, the summer monsoon over Japan and the East Asia. *J. Meteor. Soc. Japan*, **70**, 467–495.

Nitta, T., 1987: Convective activity in the tropical western Pacific and their impact on the Northern Hemisphere summer circulation. *J. Meteor. Soc. Japan*, **65**, 373–390.

Ogura, Y., T. Asai, and K. Dohi, 1985: A case study of a heavy precipitation event along the Baiu front in northern Kyushu, 23 July 1982: Nagasaki heavy rainfall. *J. Meteor. Soc. Japan*, **63**, 883–900.

Payne, A. E., and G. Magnusdottir, 2014: Dynamics of landfalling atmospheric rivers over the North Pacific in 30 years of MERRA reanalysis. *J. Climate*, **27**, 7133–7150.

Peña-Arancibia, J. L., A. I. J. M. van Dijk, L. J. Renzullo, and M. Mulligan, 2013: Evaluation of precipitation estimation accuracy in reanalyses, satellite products and an ensemble method for regions in Australia and South and East Asia. *J. Hydrometeor.*, **14**, 1323–1333.

Peixoto, J. P., and A. H. Oort, 1992: *Physics of Climate*. American Institute of Physics, New York, USA, 520 pp.

Prat, O. P., and B. R. Nelson, 2013: Mapping the world's tropical cyclone rainfall contribution over land using the TRMM multi-satellite precipitation analysis. *Water Resour. Res.*, **49**, 7236–7254.

Prat, O. P., and B. R. Nelson, 2016: On the link between tropical cyclones and daily rainfall extremes derived from global satellite observations. *J. Climate*, **29**, 6127–6135.

Ralph, F. M., P. J. Neiman, and G. A. Wick, 2004: Satellite and CALJET aircraft observations of atmospheric rivers over the eastern North Pacific Ocean during the winter of 1997/98. *Mon. Wea. Rev.*, **132**, 1721–1745.

Ralph, F. M., P. J. Neiman, G. A. Wick, S. I. Gutman, M. D. Dettinger, D. R. Cayan, and A. B. White, 2006: Flooding on California's Russian River: Role of atmospheric rivers. *Geophys. Res. Lett.*, **33**, L13801, doi:10.1029/2006GL026689.

Ralph, F. M., P. J. Neiman, G. N. Kiladis, K. Weickmann, and D. W. Reynolds, 2011: A multiscale observational case study of a Pacific atmospheric river exhibiting tropical/extratropical connections and a mesoscale frontal wave. *Mon. Wea. Rev.*, **139**, 1169–1189.

Rayner, N. A., D. E. Parker, E. B. Horton, C. K. Folland, L. V. Alexander, D. P. Rowell, E. C. Kent, and A. Kaplan, 2003: Global analyses of sea surface temperature, sea ice, and night marine air temperature since the late nineteenth century. *J. Geophys. Res.*, **108**, 4407, doi: 10.1029/2002JD002670.

Ren, F., G. Wu, W. Dong, X. Wand, Y. Wang, W. Ai, and W. Li, 2006: Changes in tropical cyclone precipitation over China. *Geophys. Res. Lett.*, **33**, L20702, doi: 10.1029/2006GL027951.

Ren, X., X.-Q. Yang, and X. Sun, 2013: Zonal oscillation of western Pacific subtropical high and subseasonal SST variations during Yangtze persistent heavy rainfall events. *J. Climate*, **26**, 8929–8946.

Row, L. W. III, D. A. Hastings, and P. K. Dunbar, 1995: *Terrainbase: Worldwide Digital Terrain Data*. NGDC Key to Geophysical Records Documentation, **30**, National Geophysical Data Center, Boulder, Colorado, USA.

Rutz, J. J., W. J. Steenburgh, and F. M. Ralph, 2014: Climatological characteristics of atmospheric rivers and their inland penetration over the western United States. *Mon. Wea. Rev.*, **142**, 905–921.

Sampe, T., and S.-P. Xie, 2010: Large-scale dynamics of the Meiyu-Baiu rain band: Environmental forcing by the westerly jet. *J. Climate*, **23**, 113–134.

Schneider, T., K. L. Smith, P. A. O'Gorman, and C. C. Walker, 2006: A climatology of tropospheric zonal-mean water vapor fields and fluxes in isentropic coordinates. *J. Climate*, **19**, 5918–5933.

Stohl, A., C. Forster, and H. Sodemann, 2008: Remote

sources of water vapor forming precipitation on the Norwegian west coast at 60°N—A tale of hurricanes and an atmospheric river. *J. Geophys. Res.*, **113**, D05102, doi:10.1029/2007JD009006.

Tao, S. Y., 1987: A review of recent research on the East Asian summer monsoon in China. *Monsoon Meteorology*. Chang, C.-P., and T. N. Krishnamurti (eds.), Oxford University Press, Oxford, 60–92.

Trenberth, K. E., and D. P. Stepaniak, 2003: Covariability of components of poleward atmospheric energy transports on seasonal and interannual time-scales. *J. Climate*, **16**, 3691–3705.

Ueda, H., A. Kibe, M. Saito, and T. Inoue, 2015: Snowfall variations in Japan and its linkage with tropical forcing. *Int. J. Climatol.*, **35**, 991–998.

Wang, B., R. Wu, and X. Fu, 2000: Pacific–East Asia teleconnection: How does ENSO affect East Asian climate? *J. Climate*, **13**, 1517–1536.

Wu, R., and B. Wang, 2002: A contrast of the East Asian summer monsoon–ENSO relationship between 1962-77 and 1978-93. *J. Climate*, **15**, 3266–3279.

Xie, S.-P., and S. G. H. Philander, 1994: A coupled ocean-atmosphere model of relevance to the ITCZ in the eastern Pacific. *Tellus A*, **46**, 340–350.

Xie, S.-P., K. Hu, J. Hafner, H. Tokinaga, Y. Du, G. Huang, and T. Sampe, 2009: Indian Ocean capacitor effect on Indo-western Pacific climate during the summer following El Niño. *J. Climate*, **22**, 730–747.

Xie, S.-P., Y. Du, G. Huang, X.-T. Zheng, H. Tokinaga, K. Hu, and Q. Liu, 2010: Decadal shift in El Niño influences on Indo–western Pacific and East Asian climate in the 1970s. *J. Climate*, **23**, 3352–3368.

Xie, S.-P., Y. Kosaka, Y. Du, K. Hu, J. S. Chowdary, and G. Huang, 2016: Indo-western Pacific ocean capacitor and coherent climate anomalies in post-ENSO summer: A review. *Adv. Atmos. Sci.*, **33**, 411–432.

Yang, J., Q. Liu, S.-P. Xie, Z. Liu, and L. Wu, 2007: Impact of the Indian Ocean SST basin mode on the Asian summer monsoon. *Geophys. Res. Lett.*, **34**, L02708, doi:10.10029/2006GL028571.

Yasutomi, N., A. Hamada, and A. Yatagai, 2011: Development of a long-term daily gridded temperature dataset and its application to rain/snow discrimination of daily precipitation. *Global Environ. Res.*, **15**, 165–172.

Yatagai, A., O. Arakawa, K. Kamiguchi, H. Kawamoto, M. I. Nodzu, and A. Hamada, 2009: A 44-year daily gridded precipitation dataset for Asia based on a dense network of rain gauges. *SOLA*, **5**, 137–140.

Yatagai, A., K. Kamiguchi, O. Arakawa, A. Hamada, N. Yasutomi, and A. Kitoh, 2012: APHRODITE: Constructing a long-term daily gridded precipitation dataset for Asia based on a dense network of rain gauges. *Bull. Amer. Meteor. Soc.*, **93**, 1401–1415.

Yoshida, K., and H. Itoh, 2012: Indirect effects of tropical cyclones on heavy rainfall events in Kyushu, Japan, during the Baiu season. *J. Meteor. Soc. Japan*, **90**, 377–401.

Zhu, Y., and R. E. Newell, 1998: A proposed algorithm for moisture fluxes from atmospheric rivers. *Mon. Wea. Rev.*, **126**, 725–735.